Published in final edited form as:

Cell Rep. 2016 March 1; 14(8): 1841–1849. doi:10.1016/j.celrep.2016.01.069.

c21orf59/kurly controls both cilia motility and polarization

Kimberly M. Jaffe[1,3], **Daniel T. Grimes**[1,3], **Jodi Schottenfeld-Roames**[1,3], **Michael E. Werner**[2], **Tse-shuen Ku**[1], **Sun K. Kim**[2], **Jose L. Pelliccia**[1], **Nicholas F. C. Morante**[1], **Brian J. Mitchell**[2,4], and **Rebecca D. Burdine**[1,4]

[1]Molecular Biology Department, Princeton University, Princeton, New Jersey, USA, 08544

[2]Cell and Molecular Biology, Feinberg School of Medicine, Northwestern University, Chicago, Illinois, USA, 60611

SUMMARY

Cilia are microtubule-based projections that function in the movement of extracellular fluid. This requires cilia to be: (1) motile, driven by dynein complexes and (2) correctly polarized on the surface of cells, which requires planar cell polarity (PCP). Few factors that regulate both processes have been discovered. We reveal that C21orf59/Kurly (Kur), a cytoplasmic protein with some enrichment at the base of cilia, is needed for motility; zebrafish mutants exhibit characteristic developmental abnormalities and dynein arm defects. *kur* was also required for proper cilia polarization in the zebrafish kidney and the larval skin of *Xenopus laevis*. CRISPR/Cas9 coupled with homologous recombination to disrupt the endogenous *kur* locus in *Xenopus* resulted in the asymmetric localization of the PCP protein Prickle2 being lost in mutant multi-ciliated cells. Kur also makes interactions with other PCP components including Disheveled. This supports a model wherein Kur plays a dual role in cilia motility and polarization.

Graphical abstract

[4]Correspondence should be addressed to BJM (brian-mitchell@northwestern.edu) and RDB (rburdine@princeton.edu).
[3]These authors contributed equally

Author Contributions

K.M.J., D.T.G., J.S.R., T.S.K, J.L.P. and N.F.C.M designed and performed zebrafish and cell culture experiments. M.E.W., S.K.K. and B.J.M. designed and performed *Xenopus* experiments. All authors interpreted the results. K.M.J., D.T.G., J.S-R, B.J.M., and R.D.B. wrote the paper.

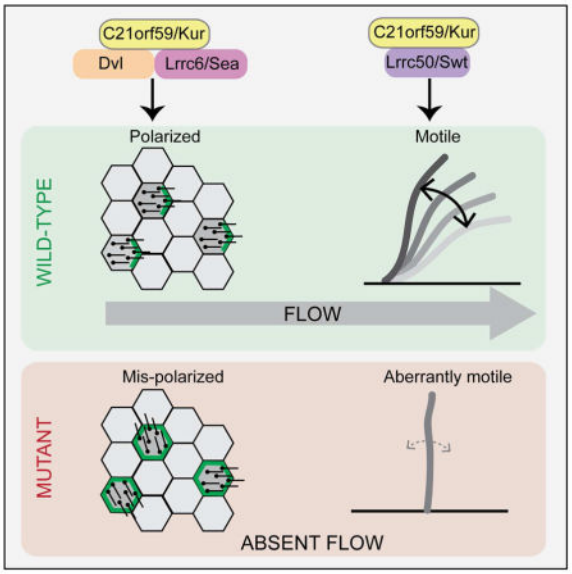

Keywords

Kurly (Kur); c21orf59; cilia; planar cell polarity; disheveled; ciliopathy; primary ciliary dyskinesia; multi-ciliated cell

Introduction

In multicellular organisms, motile cilia are present on the surface of many cell types. Their primary function is the generation of fluid flow across epithelial surfaces and, in so doing, motile cilia are required for a variety of developmental and physiological processes. As such, abnormalities in cilia-driven flow generation result in Primary Ciliary Dyskinesia (PCD), a condition that involves situs abnormalities, airway clearance defects leading to bronchiectasis, and infertility (Fliegauf et al., 2007; Norris and Grimes, 2012). In order to generate robust fluid flow, cilia must be properly motile. This requires a poorly understood pathway in which dynein arms are loaded into the cilium (Kobayashi and Takeda, 2012; Omran et al., 2008). Cilia must also be correctly positioned on the apical surface of cells (single-cell polarity) and they must be coordinately polarized across the entire tissue (tissue polarity). These roles involve the planar cell polarity (PCP) mechanism (Boutin et al., 2014; Hashimoto et al., 2010; Ohata et al., 2014; Park et al., 2008) and there also exists a feedback between cilia position and flow (Wallingford and Mitchell, 2011). To further our understanding of this link, it will be critical to discover novel components that impact cilia motility and ciliated cell PCP.

The zebrafish and *Xenopus* model systems have been used to understand the components and mechanisms required for cilia-generated fluid flow (Becker-Heck et al., 2011; Hjeij et al., 2014; Kishimoto et al., 2008; Mitchell et al., 2007; Panizzi et al., 2012; Tarkar et al., 2013; Zhao et al., 2013). Here, we describe two zebrafish mutants, called *kurly* (*kur*) that disrupt *c21orf59*, a gene recently implicated in human PCD (Austin-Tse et al., 2013). We show that Kur is involved in cilia-associated developmental processes and is required for

initiating cilia motility via recruitment of outer dynein arms (ODAs). Moreover, Kur interacts with multiple PCP components including Disheveled (Dvl) and is needed for correct cilia positioning in the zebrafish kidney. Experiments in *Xenopus*, including the generation of mosaic mutants by CRISPR/Cas9 and homologous recombination-based gene targeting, further support a role for Kur in cell polarity and tissue-level cilia polarity. Together, these results demonstrate that Kur plays a dual role in cilia motility and cilia positioning.

Results and Discussion

kur Mutants Exhibit Defects Associated with Improper Cilia-Mediated Flow Generation

kur^{tj271} and *kur*^{tm304}, two zebrafish mutants isolated from forward genetic screens (Haffter and Nusslein-Volhard, 1996), exhibit body curvature defects and kidney cysts in larval stages (Figure 1A) (Sullivan-Brown et al., 2008). The two mutations fail to complement in *trans* heterozygotes, indicating that they impact the same gene. Intriguingly, the penetrance of *kur*$^{tm304/tm304}$ mutants varied with temperature, displaying progressively more severe defects when embryos were raised at 25°C, 28°C, and 32°C, respectively (Figures 1A–B, 1D). While *kur*$^{tj271/tj271}$ mutants died as larvae, *kur*$^{tm304/tm304}$ mutants raised at the permissive temperature (25°C) often resolved their mild body curvature defects by 5 days post fertilization (dpf) or earlier (Figures 1A–B). Though kidney cysts were apparent in *kur*$^{tm304/tm304}$ embryos raised at permissive temperature, they could still be raised to adulthood. Crosses between adult homozygous *kur*$^{tm304/tm304}$ mutants suggested that male mutants are largely sterile whereas female mutants are fertile (Figure 1C). Both *kur* alleles also exhibited defects in the establishment of left-right (L-R) asymmetry. *In situ* hybridization (ISH) for genetic markers of the heart (*myl7*), liver (*fkd2*), and pancreas (*ins*) at 48 hours post fertilization (hpf) revealed incidences of reversed or randomized organ positioning (heterotaxia) with respect to normal L-R asymmetry (Figures 1D; S1D–I). *kur*$^{tj271/tj271}$ and *kur*$^{tm304/tm304}$ (raised at 28°C, as is always the case unless otherwise specified) exhibited similar L-R defects but embryos deficient for maternal and zygotic contributions of *kur* (MZ*tm304*) were slightly more affected (Figure 1D), implying a partial role for maternally supplied *kur* gene product in the control of L-R patterning. Similar to body curvature defects, lowering the incubation temperature to 25°C resulted in less severe L-R defects in MZ*kur*$^{tm304/tm304}$ mutants (Figure 1D). Organ asymmetry is governed by motile cilia-driven fluid flow within a spherical and transient structure called Kupffer's vesicle (KV) (Amack, 2014). Asymmetric flow acts to initiate a left side-restricted Nodal cascade in which expression of the zebrafish Nodal gene *southpaw* (*spaw*) and its inhibitor *lefty2* (*lft2*) are induced on the left (Nakamura and Hamada, 2012). In line with the defects in organ asymmetry, both *kur* mutants exhibited abnormalities in the asymmetric expression of *spaw* and *lft2* (Figures S1A–C, J). Together, these data place the primary L-R defect in *kur* mutants upstream of asymmetric gene expression, likely within the KV itself. Immunostaining demonstrated that cilia were present within the KV of *kur*$^{tj271/tj271}$ and MZ*kur*$^{tm304/tm304}$ mutants (Figure 1E and data not shown). At the 8 ss, we quantified the length of cilia in *kur*$^{tj271/tj271}$ mutants (n=4 embryos) and found that they were not statistically different to wild-type (n=3 embryos) controls (wild-type: 4.4 ± 0.3 μm; and *kur*$^{tj271/tj271}$: 4.4 ± 0.1 μm). Moreover, the total number of cilia per KV was unchanged in

mutants (wild-type: 60 ± 12; and $kur^{tj271/tj271}$: 69 ± 15). Thus, the generation of cilia themselves is not perturbed in *kur* mutants. However, since L-R patterning defects, kidney cysts, infertility and body curvature abnormalities are all hallmarks of abnormal cilia function in zebrafish (Sullivan-Brown et al., 2008; Yuan and Sun, 2013), we hypothesized that *kur* was required for proper flow generation by impacting cilia motility and/or cilia polarity.

kur Disrupts *c21orf59*, a Human PCD Locus

We mapped the *kur* mutations to a region on Chromosome 10 (Figure S2A). Sequencing of candidate genes revealed mutations in *c21orf59*, a gene of unknown function that is causative in some human Primary Ciliary Dyskinesia (PCD) cases (Austin-Tse et al., 2013). PCD comprises disorders resulting from aberrant cilia motility (Zariwala et al., 2011), further supporting the hypothesis that *kur* is required for motile cilia flow generation. *c21orf59* encodes a highly conserved 290-amino acid protein with an N-terminal coiled coil (CC) domain and a C-terminal domain of unknown function (DUF) (Figure 1F). kur^{tm304} harbors a point mutation at amino acid 44 (I44N) that causes either decay or instability of the protein at higher temperatures (Figures 1F and S2B), thereby serving to explain the temperature-sensitivity exhibited by $kur^{tm304/tm304}$ mutants. By contrast, the kur^{tj271} mutation introduces a stop codon at amino acid 225 (Q225X) that severely truncates the protein and results in a loss of *c21orf59* RNA (data not shown), likely due to nonsense-mediated decay (Figures 1F).

Three lines of evidence confirmed that mutations in *c21orf59* cause the *kur* phenotypes. First, antisense morpholino oligonucleotide (MO)-mediated knockdown (KD) of endogenous *c21orf59* phenocopied *kur* mutants. Morphants exhibited body curvature defects, kidney cysts, and L-R defects (Figures S2C–D). Second, injection of either human or zebrafish *c21orf59* RNA at the 1-cell stage rescued the body curvature defects of both *kur* mutants and *c21orf59* morphants; variable rescue of kidney cysts was also apparent (Figure S2C). Third, an independent study which also knocked-down *c21orf59* reported similar gross phenotypes to those exhibited by *kur* mutants (Austin-Tse et al., 2013). Thus, loss-of-function (LOF) mutations in *c21orf59* underlie the phenotypes observed in *kur* mutants. We hereafter refer to *c21orf59* as *kur*.

Kur is a Cytoplasmic Protein Required for the Initiation of Cilia Motility and Incorporation of Outer Dynein Arms in Cilia

In line with the phenotypic evidence that *kur* is needed for cilia function, *kur* RNA was present in tissues that exhibit motile cilia including the pronephric tubules and duct (PD), the dorsal forerunner cells (DFCs), KV, as well as the floor plate of the neural tube (NT) and otic vesicles (Figure 1G). In the pronephric tubules, *kur* exhibited the same staining pattern as *rfx2* and *cetn2*, markers of multi-ciliated cells (MCCs) (Figure 1G). Moreover, *kur* RNA was present at the 1-cell stage (Figure 1G), showing that the early embryo receives a maternal contribution of *kur*, a finding which can serve to explain the slightly more severe defects in MZ$kur^{tm304/tm304}$ compared to Z$kur^{tm304/tm304}$ mutants (Figure 1D).

Next, we analyzed cilia motility in *kur* mutants. Cilia in the kidney tubules and NT were almost entirely immotile in *kur*$^{tj271/tj271}$ mutants, whereas *kur*$^{tm304/tm304}$ mutants exhibited variable motility defects with greater numbers of immotile cilia observed when embryos were raised at higher temperatures (Supplementary Movies S1–S3). Changing the incubation temperature of *kur*$^{tm304/tm304}$ mutants from 25°C to 32°C did not hinder the motility of cilia that had already begun beating in the NT or kidney after 2–24 hours at the restrictive temperature (n=4/4 embryos for each location). By contrast, lowering the temperatures from 32°C to 25°C did allow immotile cilia to become motile after 12 hours (Supplementary Movie S4). A subset of immotile cilia in the KV of 28°C-raised *kur*$^{tm304/tm304}$ mutants became motile after shifting to 25°C for 70 minutes (n=2/6 embryos). After 240 minutes at 25°C, 50% of embryos harbored motile cilia in the KV (n=3/6 embryos). Furthermore, whilst embryos raised at 32°C had immotile cilia in the NT and kidney, all embryos exhibited motile cilia in these locations after an overnight incubation at 25°C (n=4/4 embryos). Together, these findings suggest that Kur is required for the initiation of motility but not its maintenance. It is noteworthy that in *Chlamydomonas reinhardtii*, an upregulation of FBB18 (the Kur homolog) was observed upon deflaggelation (Li et al., 2004), while FBB18 was stabilized upon impairment of cilia motility (Austin-Tse et al., 2013), as might be expected for a protein whose function is to aid in the initiation of cilia motility. Ultra-structural analysis revealed a lack of outer dynein arms (ODAs) in *kur*$^{tj271/tj271}$ and *kur*$^{tm304/tm304}$ mutants (Figures 2A–D), which can explain the motility defects. In accordance, *kur* morphants also exhibit ODA defects (Austin-Tse et al., 2013). Interestingly, human PCD patients harboring *C21ORF59* mutations exhibit both ODA and IDA defects.

Given these data, one possibility is that Kur controls cilia motility by participating in the assembly of ODAs in the cytoplasm and/or by assisting in the transport of ODAs into the cilium as is known to be the case for a small number of other proteins (Kobayashi and Takeda, 2012). Several lines of evidence support this view. First, epitope-tagged Kur localized to the cytoplasm in puncta, but not the cilium, in both NIH-3T3 fibroblasts (primary cilia) and KV of zebrafish embryos (motile cilia) (Figures 2F–I), similar to what has recently been described for rat tracheal cells (Austin-Tse et al., 2013). The finding that the *Chlamydomonas* Kur homolog FBB18 was stabilized upon loss of cilia motility (Austin-Tse et al., 2013) may explain our observations that Kur was undetectable in normal KV motile cilia. Second, *kur*$^{tj271/tj271}$ mutants strongly phenocopy zebrafish *switch hitter* (*swt*) mutants that harbor a mutation in *leucine rich repeat-containing 50* (*lrrc50*), a homolog of *Chlamydomonas oda7* that acts to transport intact dyneins into the cilium (Freshour et al., 2007). Third, immunoprecipitation (IP) experiments revealed a physical interaction between Kur and Lrrc50/Swt, suggesting that the proteins function in a common mechanism (Figure 2E). Thus, Kur is a cytoplasmic factor that, along with Lrrc50/Swt, likely plays a role in either the cytoplasmic pre-assembly and/or transport to the cilium of dynein complexes, potentially acting as a chaperone in the transport of dynein complexes to cilia to initiate cilia motility. Indeed, like FBB18, several other chaperones are upregulated quickly upon deflagellation in *Chlamydomonas* including Hsp70, Hsp90, and Hsp22 (Li et al., 2004).

Kur is Required for Cilia Positioning and MCC polarity

During our analysis of *kur* mutants, we noted that cilia within kidney tubules were disorganized (Figures 3A–F). The non-canonical Wnt or PCP mechanism has been implicated in the polarization of cilia (Wallingford and Mitchell, 2011). No gross convergent-extension (CE) defects, a hallmark of aberrant PCP, were observed in *kur* mutants, a result likely explained by *kur* not being expressed in a spatio-temporal manner that would be consistent with a role during gastrulation. We therefore hypothesized that Kur plays a role in PCP in ciliated cells where *kur* is expressed at high levels. To test this prediction, we first focused on the larval kidney. The kidney tubules of *kur* mutants were dilated and the cilia within were improperly oriented (Figures 3G–I and S3). Tubule dilation is common in mutants in which cilia motility is disrupted, however, other mutants that exhibit cilia motility defects and tubule dilation, such as *swt* (Figure 3L and S3) and *lok* (Figure S3) (Sullivan-Brown et al., 2008), do not exhibit polarization defects. Thus, polarization and motility are mechanistically separable and the aberrant polarization of cilia in *kur* kidney tubules is not likely a secondary consequence of motility defects or tubule dilation. As with other phenotypes reported above, cilia polarization defects in kidney tubules were temperature sensitive in $kur^{tm304/tm304}$ mutants, with more severe defects observed when embryos were raised at 32°C compared to 25°C (Figures 3G–I and S3). Embryos raised at 28°C had an intermediate phenotype (Figure 3H and S3). Raising the temperature from 25°C to 32°C did not impact the polarization of cilia (compare Figure 3J with 3G and 3I) even after an extended period at 32°C. By contrast, lowering the temperature from 32°C to 25°C did allow some recovery in cilia polarization, with more cilia being correctly polarized after the temperature was lowered (compare Figure 3K with 3G and 3I). Thus, similar to cilia motility, *kur* function appears to be required to establish, but not maintain, cilia polarity.

We next asked whether Kur has a conserved role in cilia polarity and so turned to the ciliated skin of the *Xenopus laevis* embryo, where cilia polarization is particularly well characterized (Mitchell et al., 2009). The larval skin contains numerous MCCs which possess cilia that beat in a coordinated fashion to drive directional fluid flow across the surface of the tissue. While a GFP-tagged version of *Xenopus* Kur was found to be primarily cytoplasmic, it was also enriched at the ciliary basal body and adjacent rootlet that projects away from the basal body (Figure 3M). This localization was strikingly reminiscent of Disheveled (Dvl2), an intracellular mediator of PCP signals (Park et al., 2008). *Xenopus* contains two pseudo alleles of *kur*, designated as “long” and “short” (Matsuda et al., 2015). MO-mediated KD of *kur* in *Xenopus* using both splice site and start site MOs that target both pseudo alleles of *kur* (SPL MO and ATG MO1, respectively), resulted in a complete loss of cilia-driven fluid flow along the anterior-posterior embryonic axis, consistent with a defect in cilia motility (Figure 3N). This loss of flow was partially rescued by the addition of GFP-Kur-encoding RNA that was resistant to targeting by the MO (Figure 3N).

Next, to investigate the potential effect of Kur KD on PCP, we scored the localization of the PCP component Prickle2 by imaging an exogenously supplied Prickle2-GFP which is known to asymmetrically accumulate on the posterior cell boundary of MCCs (Figure 3O) (Butler and Wallingford, 2015). Depletion of Kur using three different MOs all resulted in

uniform distribution of Prickle2-GFP relative to membrane-associated RFP (memRFP) (Figure 3O), suggesting a loss in proper PCP. Importantly, this loss of Prickle2-GFP asymmetry was largely rescued by the expression of *kur* RNA (Figure 3O). Polarity of MCC cilia arises from a combination of PCP coupled to a positive feedback mechanism driven by flow-mediated hydrodynamic forces (Mitchell et al., 2007; Mitchell et al., 2009; Park et al., 2008). Interestingly, a third MO (ATG MO2), targeting only one *kur* allele (the "long" allele), resulted in a weaker flow phenotype (Figure 3N) and maintained normal cilia beat frequency (control, 17.8 ± 1.3 Hz; and Kur ATG MO2, 18.4 ± 2.8 Hz). Thus, in this morphant, the decrease in flow could result from either a loss of cilia polarity (within the cell) or a loss of MCC polarity (within the tissue). To distinguish between these possibilities we assessed cilia polarity in ATG MO2 morphants, finding that whilst cilia were coordinately polarized within individual MCCs, there was a loss of coordinated polarity between MCCs (Figures S4D–E). In control embryos, 95% of cells orient their cilia in the posterior direction, thus facilitating the generation of a robust, posteriorly-directed fluid flow. By contrast, *kur* KD (ATG MO2) led to a significant number of cells mispolarizing in the anterior direction (Figure S4E) This phenotype is consistent with a defect in PCP signaling and is similar to what has been reported for manipulations of the Wnt receptor Frizzled-3 and the PCP component Vangl2 (Figure S4E) (Mitchell et al., 2009).

To further validate the Kur depletion phenotype we used CRISPR/Cas9-mediated genome editing in combination with homologous recombination (HR)-induced integration (Auer and Del Bene, 2014) to generate mosaic F0 mutant animals. A single guide RNA (gRNA) was designed to induce double strand breaks in both long and short alleles of the *kur* gene. We co-injected the gRNA/Cas9 with allele-specific DNA targeting constructs containing a fluorescent marker such that cells edited for the long allele integrated BFP with a terminal codon and cells edited for the short allele integrated RFP with a terminal codon (Figure S4A–B). Gene targeting was confirmed by PCR (Figure S4C). In MCCs containing both BFP and RFP, we observed a complete loss of Prickle2-GFP asymmetric localization, similar to what was observed in the *kur* morphants (Figure 3P). Interestingly, cells that contained either BFP or RFP, indicating editing of only a single allele, gave an intermediate phenotype in which the Prickle2-GFP asymmetry was still present but considerably weaker (Figure 3P).

The loss of MCC cilia polarity coupled with the loss of Prickle2 asymmetry when *kur* is knocked-down or mutated indicates that Kur has an important role in facilitating the establishment of cilia polarity. Furthermore, our results indicate that the function of Kur in cilia motility can be separated from its role in PCP.

Kur Makes Interactions with PCP Components and Represses the Canonical Wnt Pathway

Given the polarity defects exhibited by *kur* mutants and morphants, we searched for interactions between Kur and known PCP pathway components. *kur* zebrafish mutants strongly phenocopy *inversin* (*inv*) morphants, with both exhibiting kidney cysts, L-R patterning defects, and aberrant body curvature (Simons et al., 2005). Inv is thought to act as a molecular switch controlling the relative activities of canonical Wnt and PCP signaling by interacting with and modulating the function of Dvl (Simons et al., 2005). We tested for a

genetic interaction between *kur* and *inv* by injecting suboptimal doses of MOs targeting these genes. In this experiment, targeting of *inv* or *kur* alone produced minimal body curvature defects and few kidney cysts (Figures 4A–B). However, co-injection of these MOs at the same doses produced much more striking body curvature and kidney cyst phenotypes (Figures 4A–B) that were significantly different to single injected embryos or uninjected controls (Figure 4C). This suggests that *kur* genetically interacts with *inv* to modulate common processes.

Given these genetic findings, we then asked whether Kur protein physically associates with members of the PCP pathway. By co-IP of tagged proteins, we found that Kur and Dvl physically interact (Figure 4D). Dvl consists of three distinct domains: a DIX domain that controls canonical Wnt signaling as well as DEP and PDZ domains that play roles in PCP. Utilizing Dvl deletion constructs, we found that Kur interacted with both the DEP and PDZ domains but we could not detect an interaction between Kur and the DIX domain (Figure 4E). Moreover, Kur also associated with Leucine rich repeat containing-6 (Lrrc6/Seahorse (Sea)) (Figure 4F), another Dvl-interacting protein that controls the switch between canonical Wnt and PCP signaling (Kishimoto et al., 2008; Serluca et al., 2009). Intriguingly, Sea has also been implicated in the regulation of cilia motility by control of dynein arm assembly (Serluca et al., 2009; Zhao et al., 2013). In conclusion, the genetic and physical interactions between Kur and known PCP components, together with the polarity defects of *kur* mutants and morphants, strongly supports a role for Kur in controlling polarity via PCP.

Finally, we reasoned that if Kur promotes PCP signals then it might act as a repressor of canonical Wnt signaling. Using luciferase readouts of the Super8XTopFlash reporter to assay Dvl's ability to activate canonical Wnt signaling, we found that Kur does indeed repress canonical Wnt signals (Figure S4F). While expression of Dvl alone led to strong induction of the reporter, co-expression of either Dvl/Kur or Dvl/Sea led to reduced reporter activity. Expression of Dvl, Kur, and Sea together further repressed activation of the canonical Wnt reporter (Figure S4F). Thus, Kur likely acts alongside Inv and Sea to promote PCP signaling over canonical Wnt signaling via Dvl. Crucially, defects in these pathways upon *kur* LOF would be restricted to ciliated cells where *kur* is strictly localized, explaining the lack of gross canonical Wnt phenotypes or CE defects in *kur* mutants and morphants. Finally, we performed overexpression of *kur* in zebrafish by injection of wild-type RNA at the 1-cell stage. Injection of *kur* RNA induced moderate dorsalization (Figure S4G). In agreement with the Super8XTopFlash reporter assay, this suggests that Kur can act as a repressor of canonical Wnt.

Together, these findings from zebrafish and *Xenopus* demonstrate that Kur is involved in both cilia motility and polarization to control cilia-mediated processes such as the generation of fluid flow. As the role for the Kur homolog FBB18 in cilia motility is conserved in *Chlamydomonas* (Li et al., 2004), we suggest that this was the ancestral function of Kur and that its interactions with the PCP pathway evolved later along with multicellularity. Given the multitude of physical interactions Kur makes with proteins required for cilia motility and PCP, we propose that Kur acts as a scaffold to coordinate the activity of these two pathways. Indeed, by being involved in both cilia motility and ciliated cell PCP, Kur is a good candidate for a gene that mechanistically links these two processes which are both critical

for cilia function and the generation of polarized fluid flow. It will be important to find more components of these pathways, and to further characterize these processes at the molecular level, to aid in the understanding and diagnosis of human conditions such as PCD.

Experimental Procedures

Zebrafish Mutants

kur^{tj271} and *kur*^{tm304} originated as part of a large-scale ENU mutagenesis screen (Haffter et al., 1996). They were generated in the TU strain and maintained by outcrossing to AB, WIK, and PWT. MZ*kur*^{tm304} embryos were obtained by crossing a *kur*$^{tm304/tm304}$ female with a *kur*$^{+/tm304}$ male as homozygous males are sterile. Embryos were maintained at 28°C unless otherwise specified.

CRISPR/Cas9-Mediated Homologous Recombination in *Xenopus laevis*

kur mutant cells were generated in F0 animals using CRISPR/Cas9-mediated genome editing. A guide RNA (GAGGCCACAGACCAGCTGAG[GGG]) that targeted both pseudo alleles of *Xenopus kur* (Xl.4468) was designed (Chr2L:14433422-14433441 and Chr2S: 19471649-19471627). Homologous recombination (HR) facilitated “repair” was performed using ~400 bp homology arms such that BFP was inserted in frame into the “long” Chr2L pseudo allele (with a terminal stop codon) and RFP was inserted in frame into the “short” Chr2S allele (with a terminal stop codon) to mark cells that were edited (Figure S4A–B). Fertilized eggs were injected at the 1 cell stage with 500 pg Cas9 protein (PNAbio, CP01-250), 500 pg sgRNA, and 25 pg each of the circular plasmid DNA containing the homology arms and fluorescent marker (pKHR-Kur2L-BFP and pKHR-Kur2S-RFP). While the F0 animals are mosaic, the DNA containing the homology arms and the fluorescent markers has no promoter such that edited cells are the only cells that fluoresce (note: Kur is expressed in MCCs, therefore fluorescent expression specific to MCCs is further evidence of proper insertion). The presence of BFP and RFP insertions was verified using PCR to amplify fragments using BFP or RFP primers and primers outside of the homology arms (Figure S4A–C). Using this approach, we scored the fluorescent intensity (see below) of Prickle2-GFP in cells that were fluorescent for either BFP, RFP, or both BFP and RFP.

Supplementary Material

Refer to Web version on PubMed Central for supplementary material.

Acknowledgments

The authors thank: Derrick Bosco, Cori Hasty, Phillip Johnson, Heather McAllister and LAR staff for zebrafish care, Ray Habas for Dvl constructs, K. Horvath for Renilla constructs, and Dr. Gary Laevsky and the Molecular Biology Confocal Microscopy Facility which is a Nikon Center of Excellence. This research was supported in part by a competitive research award to BJM from the Eugene and Millicent Bell Fellowship Fund in Tissue Engineering and the Laura and Arthur Colwin Endowed Summer Research Fellowship Fund at the Marine Biological Laboratory in Woods Hole, MA. The research was also supported by an NRSA grant to K.M.J (#1F32HD060396-01A1), an NIH-NIGMS grant to B.J.M. (#2R01GM089970) and an NIH-NICHD grant to R.D.B. (#2R01HD048584).

References

Amack JD. Salient features of the ciliated organ of asymmetry. Bioarchitecture. 2014; 4:6–15. [PubMed: 24481178]

Auer TO, Del Bene F. CRISPR/Cas9 and TALEN-mediated knock-in approaches in zebrafish. Methods. 2014; 69:142–150. [PubMed: 24704174]

Austin-Tse C, Halbritter J, Zariwala MA, Gilberti RM, Gee HY, Hellman N, Pathak N, Liu Y, Panizzi JR, Patel-King RS, et al. Zebrafish Ciliopathy Screen Plus Human Mutational Analysis Identifies C21orf59 and CCDC65 Defects as Causing Primary Ciliary Dyskinesia. American journal of human genetics. 2013; 93:672–686. [PubMed: 24094744]

Becker-Heck A, Zohn IE, Okabe N, Pollock A, Lenhart KB, Sullivan-Brown J, McSheene J, Loges NT, Olbrich H, Haeffner K, et al. The coiled-coil domain containing protein CCDC40 is essential for motile cilia function and left-right axis formation. Nature genetics. 2011; 43:79–84. [PubMed: 21131974]

Boutin C, Labedan P, Dimidschstein J, Richard F, Cremer H, Andre P, Yang Y, Montcouquiol M, Goffinet AM, Tissir F. A dual role for planar cell polarity genes in ciliated cells. Proceedings of the National Academy of Sciences of the United States of America. 2014; 111:E3129–3138. [PubMed: 25024228]

Butler MT, Wallingford JB. Control of vertebrate core planar cell polarity protein localization and dynamics by Prickle 2. Development (Cambridge, England). 2015; 142:3429–3439.

Fliegauf M, Benzing T, Omran H. When cilia go bad: cilia defects and ciliopathies. Nature reviews. 2007; 8:880–893.

Freshour J, Yokoyama R, Mitchell DR. Chlamydomonas flagellar outer row dynein assembly protein ODA7 interacts with both outer row and I1 inner row dyneins. The Journal of biological chemistry. 2007; 282:5404–5412. [PubMed: 17194703]

Haffter P, Nusslein-Volhard C. Large scale genetics in a small vertebrate, the zebrafish. The International journal of developmental biology. 1996; 40:221–227. [PubMed: 8735932]

Hashimoto M, Shinohara K, Wang J, Ikeuchi S, Yoshiba S, Meno C, Nonaka S, Takada S, Hatta K, Wynshaw-Boris A, et al. Planar polarization of node cells determines the rotational axis of node cilia. Nature cell biology. 2010; 12:170–176. [PubMed: 20098415]

Hjeij R, Onoufriadis A, Watson CM, Slagle CE, Klena NT, Dougherty GW, Kurkowiak M, Loges NT, Diggle CP, Morante NF, et al. CCDC151 mutations cause primary ciliary dyskinesia by disruption of the outer dynein arm docking complex formation. American journal of human genetics. 2014; 95:257–274. [PubMed: 25192045]

Kishimoto N, Cao Y, Park A, Sun Z. Cystic kidney gene seahorse regulates cilia-mediated processes and Wnt pathways. Developmental cell. 2008; 14:954–961. [PubMed: 18539122]

Kobayashi D, Takeda H. Ciliary motility: the components and cytoplasmic preassembly mechanisms of the axonemal dyneins. Differentiation; research in biological diversity. 2012; 83:S23–29.

Li JB, Gerdes JM, Haycraft CJ, Fan Y, Teslovich TM, May-Simera H, Li H, Blacque OE, Li L, Leitch CC, et al. Comparative genomics identifies a flagellar and basal body proteome that includes the BBS5 human disease gene. Cell. 2004; 117:541–552. [PubMed: 15137946]

Matsuda Y, Uno Y, Kondo M, Gilchrist MJ, Zorn AM, Rokhsar DS, Schmid M, Taira M. A New Nomenclature of Xenopus laevis Chromosomes Based on the Phylogenetic Relationship to Silurana/Xenopus tropicalis. Cytogenetic and genome research. 2015; 145:187–191. [PubMed: 25871511]

Mitchell B, Jacobs R, Li J, Chien S, Kintner C. A positive feedback mechanism governs the polarity and motion of motile cilia. Nature. 2007; 447:97–101. [PubMed: 17450123]

Mitchell B, Stubbs JL, Huisman F, Taborek P, Yu C, Kintner C. The PCP pathway instructs the planar orientation of ciliated cells in the Xenopus larval skin. Curr Biol. 2009; 19:924–929. [PubMed: 19427216]

Nakamura T, Hamada H. Left-right patterning: conserved and divergent mechanisms. Development (Cambridge, England). 2012; 139:3257–3262.

Norris DP, Grimes DT. Mouse models of ciliopathies: the state of the art. Disease models & mechanisms. 2012; 5:299–312. [PubMed: 22566558]

Ohata S, Nakatani J, Herranz-Perez V, Cheng J, Belinson H, Inubushi T, Snider WD, Garcia-Verdugo JM, Wynshaw-Boris A, Alvarez-Buylla A. Loss of Dishevelleds disrupts planar polarity in ependymal motile cilia and results in hydrocephalus. Neuron. 2014; 83:558–571. [PubMed: 25043421]

Omran H, Kobayashi D, Olbrich H, Tsukahara T, Loges NT, Hagiwara H, Zhang Q, Leblond G, O'Toole E, Hara C, et al. Ktu/PF13 is required for cytoplasmic pre-assembly of axonemal dyneins. Nature. 2008; 456:611–616. [PubMed: 19052621]

Panizzi JR, Becker-Heck A, Castleman VH, Al-Mutairi DA, Liu Y, Loges NT, Pathak N, Austin-Tse C, Sheridan E, Schmidts M, et al. CCDC103 mutations cause primary ciliary dyskinesia by disrupting assembly of ciliary dynein arms. Nature genetics. 2012; 44:714–719. [PubMed: 22581229]

Park TJ, Mitchell BJ, Abitua PB, Kintner C, Wallingford JB. Dishevelled controls apical docking and planar polarization of basal bodies in ciliated epithelial cells. Nature genetics. 2008; 40:871–879. [PubMed: 18552847]

Serluca FC, Xu B, Okabe N, Baker K, Lin SY, Sullivan-Brown J, Konieczkowski DJ, Jaffe KM, Bradner JM, Fishman MC, et al. Mutations in zebrafish leucine-rich repeat-containing six-like affect cilia motility and result in pronephric cysts, but have variable effects on left-right patterning. Development (Cambridge, England). 2009; 136:1621–1631.

Simons M, Gloy J, Ganner A, Bullerkotte A, Bashkurov M, Kronig C, Schermer B, Benzing T, Cabello OA, Jenny A, et al. Inversin, the gene product mutated in nephronophthisis type II, functions as a molecular switch between Wnt signaling pathways. Nature genetics. 2005; 37:537–543. [PubMed: 15852005]

Sullivan-Brown J, Schottenfeld J, Okabe N, Hostetter CL, Serluca FC, Thiberge SY, Burdine RD. Zebrafish mutations affecting cilia motility share similar cystic phenotypes and suggest a mechanism of cyst formation that differs from pkd2 morphants. Developmental biology. 2008; 314:261–275. [PubMed: 18178183]

Tarkar A, Loges NT, Slagle CE, Francis R, Dougherty GW, Tamayo JV, Shook B, Cantino M, Schwartz D, Jahnke C, et al. DYX1C1 is required for axonemal dynein assembly and ciliary motility. Nature genetics. 2013; 45:995–1003. [PubMed: 23872636]

Wallingford JB, Mitchell B. Strange as it may seem: the many links between Wnt signaling, planar cell polarity, and cilia. Genes & development. 2011; 25:201–213. [PubMed: 21289065]

Yuan S, Sun Z. Expanding horizons: ciliary proteins reach beyond cilia. Annual review of genetics. 2013; 47:353–376.

Zariwala MA, Omran H, Ferkol TW. The emerging genetics of primary ciliary dyskinesia. Proceedings of the American Thoracic Society. 2011; 8:430–433. [PubMed: 21926394]

Zhao L, Yuan S, Cao Y, Kallakuri S, Li Y, Kishimoto N, DiBella L, Sun Z. Reptin/Ruvbl2 is a Lrrc6/Seahorse interactor essential for cilia motility. Proceedings of the National Academy of Sciences of the United States of America. 2013; 110:12697–12702. [PubMed: 23858445]

Highlights

- *Kurly* (*kur*) mutants exhibit defects characteristic of motile cilia dysfunction
- *c21orf59* is mutated in *kur* and is needed for dynein arm localization/cilia motility
- CRISPR/Cas9 with homologous recombination in *Xenopus* shows C21orf59 regulates PCP
- C21orf59 interacts with various PCP components to correctly polarize motile cilia

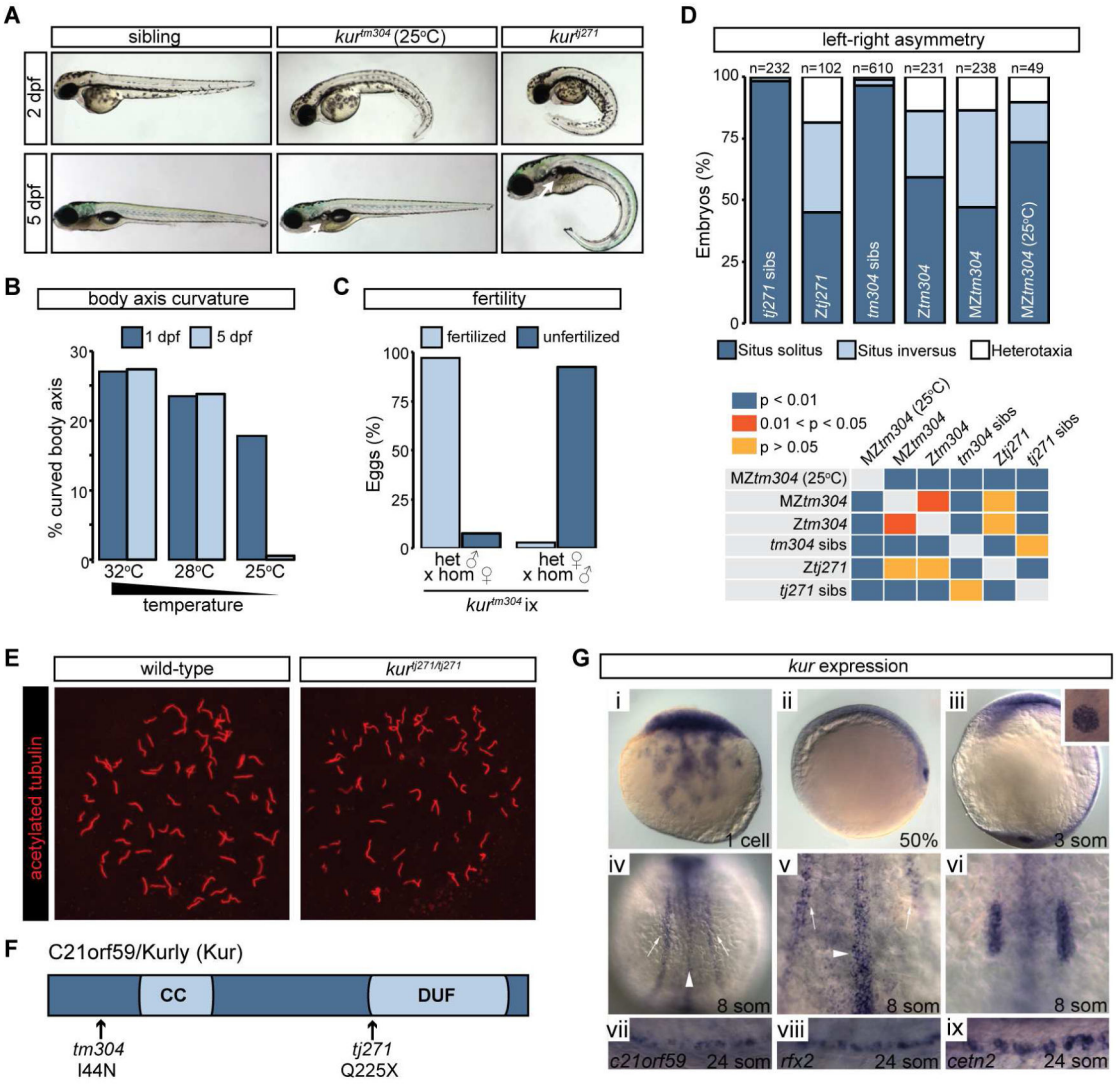

Figure 1. *kur* Mutants Harbor Mutations in *c21orf59* and Exhibit Defects Characteristic of Defective Cilia Motility

(A) Lateral views of zebrafish sibling control embryos and *kur*^{tm304} and *kur*^{tj271} mutants at 2 dpf and 5 dpf. At 25°C, *kur*^{tm304} mutants exhibit early body axis defects that resolve by 5 dpf whereas *kur*^{tj271} mutants do not resolve their body curvatures. Both mutants exhibit kidney cysts (white arrows) but the penetrance is variable in *kur*$^{tm304/tm304}$ at 25°C.

(B) Embryos from *kur*$^{+/tm304}$ intercrosses were raised at 32°C, 28°C, or 25°C and were scored for body curvature defects at 1 dpf and 5 dpf. Whilst abnormalities were present in around 25% of embryos at 32°C and 28°C, mutants raised at 25°C exhibited fewer incidences of axis curvature at 1 dpf and almost all mutants had recovered at 5 dpf. The total number of embryos examined was 32°C n=292; 28°C n=332; and 25°C n=341. Shown is the average percentage of embryos with curved body axis from 4 biological replicates.

(C) Fertility of *kur*^{tm304} adult mutants was assessed by scoring the number of fertilized eggs following homozygous female crosses to heterozygous males and vice versa. Shown is the average percentage of embryos fertilized from 3 biological replicates.

(D) Percentage of embryos showing the indicated situs phenotypes. Embryos were processed by ISH for *myl7*, *ins* and *fkd2* to mark the heart, pancreas, and liver, respectively, at 2 dpf. Statistical comparison of different genotypes was performed using chi-square analysis with $p < 0.05$ being considered to report significant differences.
(E) Early somite stage embryos were processed for immunostaining using acetylated alpha-tubulin antibodies to mark the ciliary axoneme. Confocal imaging of KV revealed the presence of cilia in sibling control embryos as well as MZ*kur*^{tm304} mutants and *c21orf59* morphants.
(F) Schematic diagram of C21orf59/Kurly (Kur) protein showing the approximate positions of the predicted coiled coil (CC) domain and the domain of unknown function (DUF). The position and nature of the *kur*^{tm304} (I44N) and *kur*^{tj271} (Q225X) mutations are shown.
(G) *kur* expression in zebrafish embryos at the stages indicated. *kur* is provided maternally at the 1-cell stage (i) followed by expression in the DFCs at 50% epiboly (ii). Expression is observed in KV (iii), pictured here at the 3-somite stage with a close-up of KV in the inset. During somitogenesis, *kur* is expressed in tissues with motile cilia including the pronephros (white arrows), the floorplate of the neural tube (white arrowheads) and the otic vesicles (iv–vi). Expression in the pronephros at the 24-somite stage overlaps with MCC markers *rfx2* and *cetn2* (vii–ix).

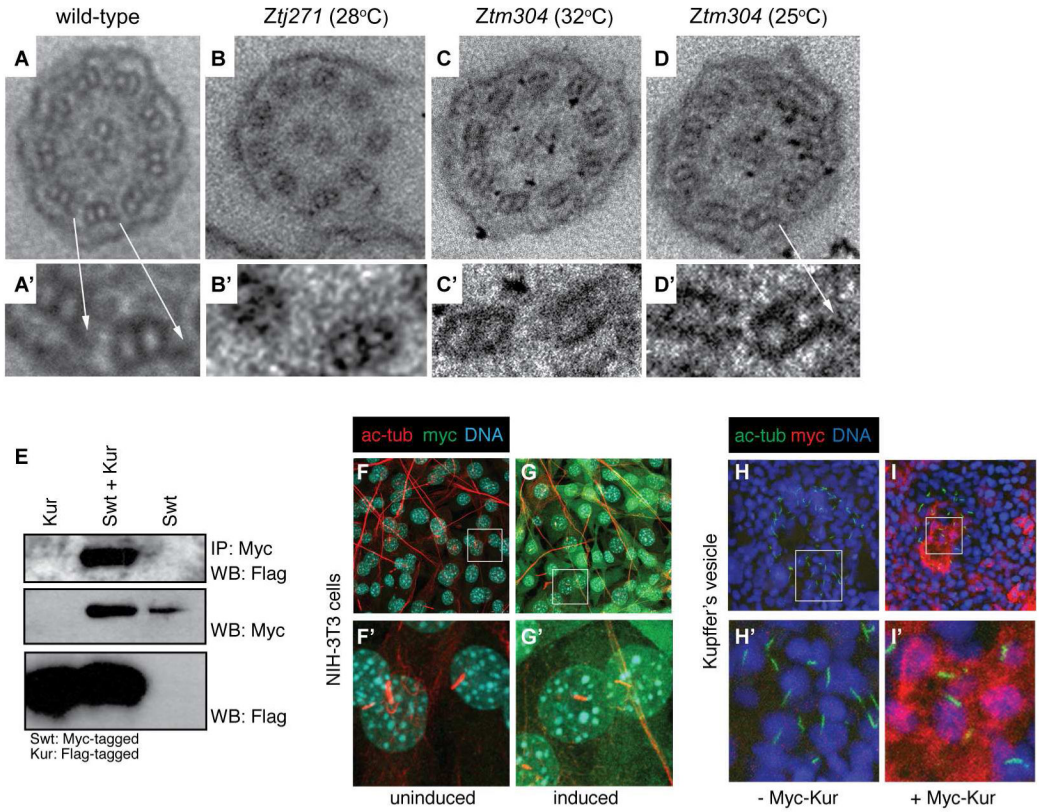

Figure 2. Kur is a Cytoplasmic Factor Required for the Localization of ODAs to the Cilium

(A–D′) Transmission electron micrographs (TEMs) showing the ultrastructure of pronephric cilia in cross-section. Arrows in A–A′ indicate outer dynein arms (ODAs) which are missing in mutants (B–C′) but are restored in *kur*$^{tm304/tm304}$ mutants raised at permissive temperature (D–D′).

(E) Immunoprecipitation (IP) of Myc-tagged Swt and subsequent Myc-Swt and Flag-Kur western blot (WB) reveals physical association between Swt and Kur.

(F–G′) NIH-3T3 cells transfected with inducible Myc-tagged Kur were immunostained for the ciliary axoneme (acetylated alpha tubulin (ac-tub); red), DNA (Hoechst; blue), and myc (Myc-Kur; green). Kur is not localized to the cilium but instead localizes to the cytoplasm.

(H–I′) Immunostaining of Kupffer's vesicle (KV) in control embryos or embryos injected with Myc-Kur. Cilia were marked by ac-tub (green) staining, DNA with Hoechst (blue), and Myc-Kur was localized with an anti-Myc antibody (red). Myc-Kur, which rescues *kur* mutants, was present in cells of the KV but appeared absent from cilia themselves.

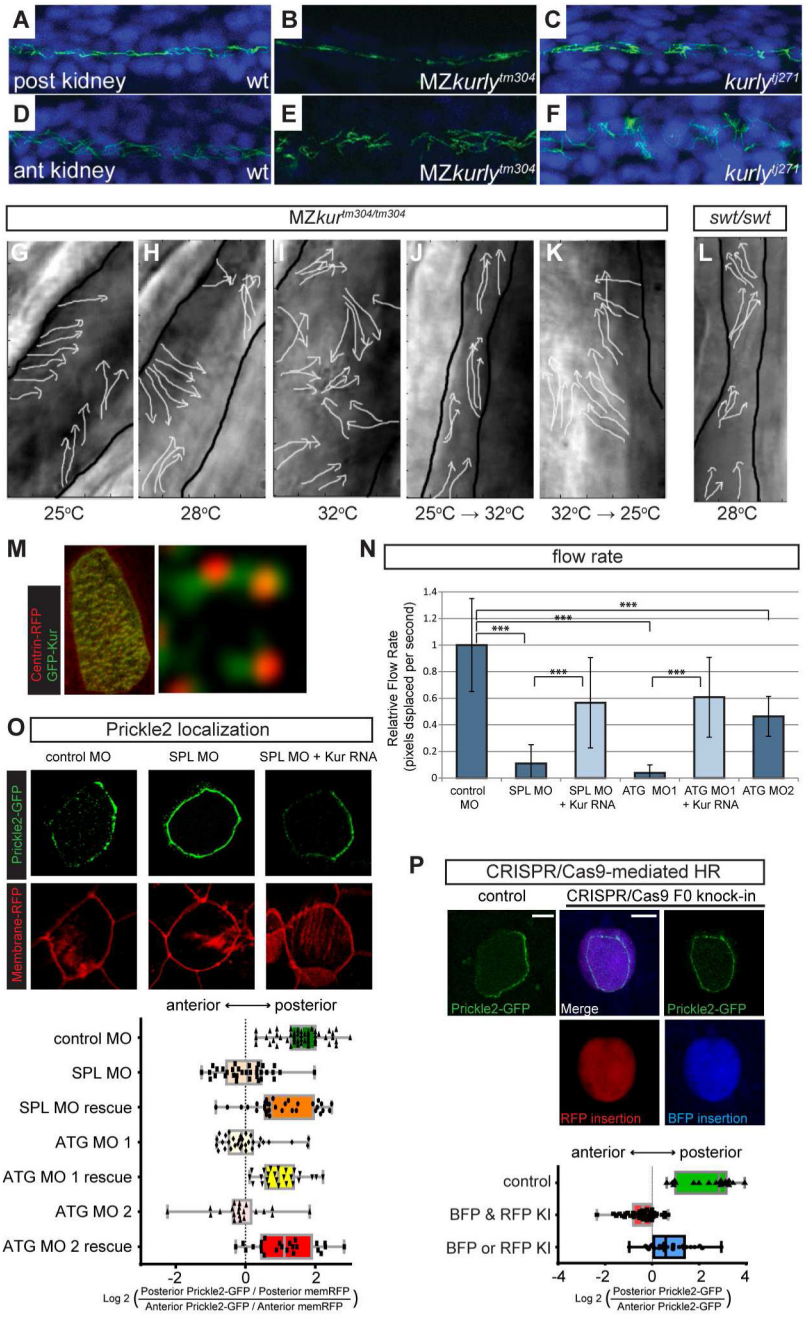

Figure 3. *kur* Mutants and Morphants Exhibit Polarity Defects in Zebrafish and *Xenopus*

(A–F) Staining of cilia axonemes (ac-tub; green) and nuclei (Hoechst; blue) in zebrafish pronephric tubules show cilia are present but appear disorganized and mispolarized in mutants.

(G–L) Stills from live imaging of cilia. Cilia directionality is traced by arrows in MZ*kur*$^{tm304/tm304}$ (G–K) and *lok*$^{to237b/to237b}$ mutants (L). Black outlines mark the edges of the tubules. Cilia in MZ*kur*$^{tm304/tm304}$ are progressively more disorganized at higher temperatures (G–I). Temperature shift experiments in *kur*$^{tm304/tm304}$ mutants show that cilia do not becoming disorganized after shifting from permissive to restrictive temperatures

(25°C→32°C) (J) and that cilia are able to recover their alignment defects by shifting from restrictive to permissive temperatures (32°C→25°C) (K). *swt/swt* mutants exhibit dilated tubules but normal cilia alignment (L), suggesting that tubule dilation does not cause alignment defects.

(M) Cytoplasmic localization of GFP-Kur in a *Xenopus* multi-ciliated cell (MCC) showing an enrichment at the basal body and rootlets (inlay).

(N) Quantification of cilia generated fluid flow in control embryos and *kur* morphants. Average flow velocity measured by the displacement of dyed micro-beads along the skin of stage 29 *Xenopus* embryos. Data represent 3 independent MOs and rescue experiments were performed with GFP-Kur RNA. Values are averages of at least 10 flow lines from 5 embryos from 2 independent experiments. Error bars indicate standard deviation, *** p value < 0.0002.

(O) Representative images and quantification of Prickle2-GFP (green) and membrane-RFP (red) localization in control and *kur* morphants (posterior is right). Box and whisker plots represent the log2 of the posterior fluorescent intensity divided by the anterior fluorescent intensity normalized for membrane-RFP (memRFP) intensity.

(P) Representative images and quantification of Prickle2-GFP localization in mosaic F0 CRISPR/Cas9-edited MCCs. Control embryos were injected Cas9 protein and homology arms without kur gRNA. RFP positive MCCs indicate integration of RFP into the short *kur* allele and BFP positive MCCs indicate integration of BFP into the long *kur* allele. Box and whisker plot represents the log2 of the posterior Prickle2-GFP fluorescent intensity divided by the anterior fluorescent intensity.

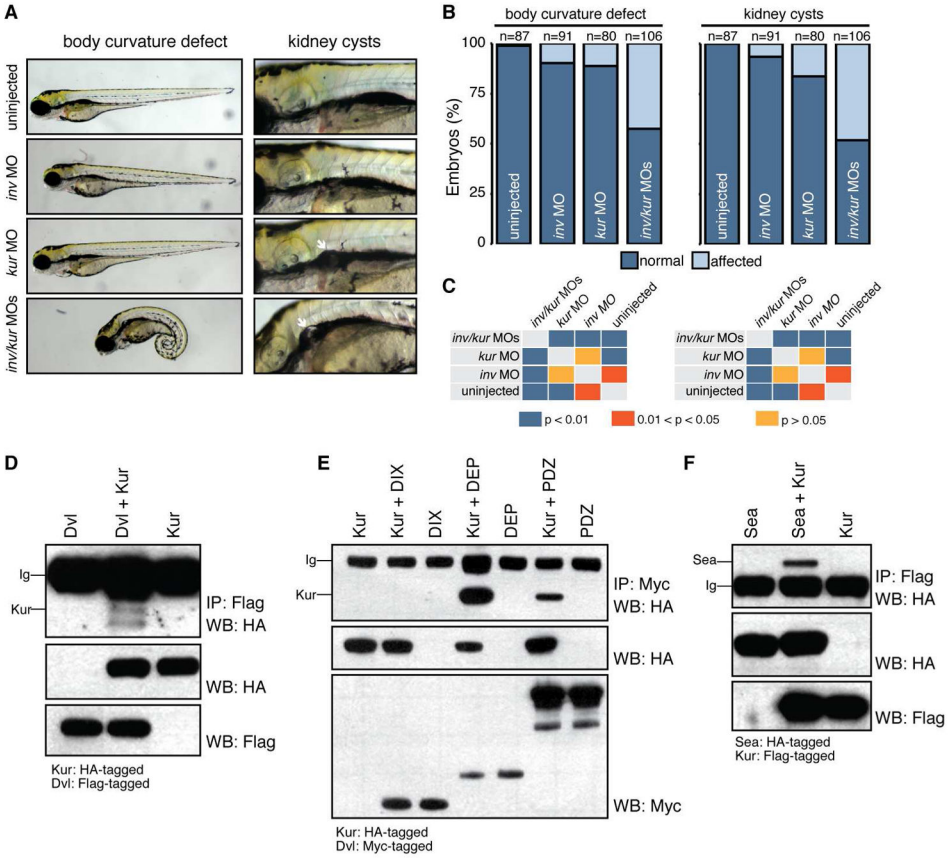

Figure 4. Kur Interacts with PCP Components

(A–C) Low concentration of *inv* or *kur* MO produce few defects but, in combination, produce additive defects in body curvature and presence of kidney cysts. White arrows show kidney cysts. Statistical comparison of different genotypes was performed using chi-square analysis with $p < 0.05$ being considered to report significant differences.

(D) Immunoprecipitation (IP) of Flag-tagged Dvl and subsequent Flag-Dvl and HA-Kur wetern blot (WB) reveals physical association between Dvl and Kur.

(E) Immunoprecipitation (IP) of Myc-tagged Dvl domains and subsequent Myc-Dvl and HA-Kur western blot (WB) reveals physical association between Kur and the DEP and PDZ domains but not the DIX domain of Dvl.

(F) Immunoprecipitation (IP) of Flag-tagged Kur and subsequent Flag-Kur and HA-Sea western blot (WB) reveals physical association between Sea and Kur.